Rain storage in forests detected with ERS tandem mission SAR

Jong, Joost de; Klaassen, Wim; Ballast, Albert

Published in:
Remote Sensing of Environment

DOI:
10.1016/S0034-4257(99)00100-5

Publication date:
2000

ELSEVIER

Rain Storage in Forests Detected with ERS Tandem Mission SAR

Joost de Jong, Wim Klaassen,* and Albert Ballast†*

Rainfall interception by vegetation is a major component in the hydrological balance at the land surface. Small-scale variations in rainfall interception occur when both rainfall and land surface are highly variable. A key parameter of interception is the amount of rain stored on vegetation. As radar backscatter is strongly influenced by the free-water content of vegetation, SAR remote sensing might be applied to analyze large-scale rainfall interception. We concentrated in this study on C-band radar and rainfall storage in forests. The backscatter sensitivity to wetness is simulated with a radiative transfer model, which has been modified to describe the changes in dimension and dielectric constant of leaves and needles due to wetting. The simulations indicate that backscatter may decrease when a sparse coniferous forest is wetted, while the backscatter of a closed forest is found to increase with 1–4 dB due to rain storage. Thus, the sensitivity to storage strongly depends on the type of forest. The simulations are empirically tested by analyzing two sets of successive SAR image pairs from the ERS tandem mission. Given the short time between these measurements, it is argued that backscatter changes are caused mainly by changes in rain storage. The observed backscatter change is compared with wetness change estimated by a standard hydrological model using ground-based rain radar observations as input. The observed backscatter change between a wet and a dry forest varied between 0.7 dB and 2.5 dB, in the range of the simulations. It is concluded that C-band SAR is sensitive to forest wetness, although for a quantitative assessment of water storage on forest additional information on at least forest structure is needed. ©Elsevier Science Inc., 2000

INTRODUCTION

Rainfall interception is defined as rain that is intercepted by vegetation and evaporated without reaching the ground (Horton, 1919; Rutter et al., 1971; Gash, 1979). Interception accounts for approximately 20% of net evaporation from the earth land surface (Choudhury et al., 1998) and for 25–40% from temperate forests (Linacre and Geerts, 1997, p. 98). It is therefore a major component in the hydrological balance at the land surface. As water vapor is the most important greenhouse gas, interception influences climate (Gates et al., 1996; Sellers et al., 1997).

Precipitation, evaporation and interception are processes occurring at a spatial scale of 5 m to 50 km (Blöschl and Sivapalan, 1995). Large-scale climatological and hydrological models have grid cells of ~1000 km^2. As a consequence, interception within a grid cell is heterogeneous. This subgrid heterogeneity strongly influences the modeled hydrological balance and climate (e.g., Shuttleworth, 1988; Pitman et al., 1990; Dolman and Gregory, 1992; Eltahir and Bras, 1993; Noilhan et al., 1997). Current approaches to account for subgrid heterogeneity are poorly validated, as only local interception measurement techniques are available. A large-scale measurement technique would therefore be a useful tool in the validation of large-scale interception models.

A key parameter in the interception process is wetness, here defined as the amount of rain stored on vegetation. Most storage occurs on the foliage, where rain forms a water layer on hydrophilic leaves or drops on hydrophobic leaves (Horton, 1919). The backscatter measured by a Synthetic Aperture Radar (SAR) is positively related to the water content of the vegetation cover, and therefore a SAR might be able to quantify

*Department of Physical Geography, University of Groningen, The Netherlands

†Department of Physics, University of Groningen, The Netherlands

Address correspondence to Joost de Jong, University of Groningen, Department of Physical Geography, Kerklaan 30, 9751 NN Haren, The Netherlands. E-mail: j.j.m.de.Jong@biol.rug.nl

Received 5 April 1999; revised 12 September 1999.

REMOTE SENS. ENVIRON. 72:170–180 (2000)

655 Avenue of the Americas, New York, NY 10010

0034-4257/00/$–see front matter
PII S0034-4257(99)00100-5

large-scale rain storage. C-band backscatter of forests increases up to 3 dB shortly after rainfall (e.g., Bernard and Vidal-Madjar, 1989; Way et al., 1990; Dobson et al., 1991; Ahern et al., 1993; Pulliainen et al., 1994; Rignot et al., 1994). On the other hand, a slight backscatter decrease is also observed for a wet coniferous forest (Schowengerdt, 1983) and densely vegetated agricultural areas (Bergen et al., unpublished). The mechanisms causing the observed backscatter change after rainfall are still poorly understood (Hobbs et al., 1998; Saich and Borgeaud, 1998). Uncertainty arises, as the recorded total backscatter is not only influenced by the water stored on top of the vegetation but also by moisture and structure of both soil and vegetation.

A promising approach to singling out the factor rain storage on vegetation is backscatter change detection between successive days with a wet and a dry vegetation cover. The vegetation and soil structure can be assumed to be unchanged. Moreover, this method may distinguish between the quick drying of the vegetation and the slow drying of the underlying soil. Preliminary model calculations indicate that the backscatter change of a forest with a wet and a dry canopy varies between 0.5 and 1.8 dB for the C-band (Klaassen et al., 1997).

The feasibility of measuring large-scale rain storage by SAR with successive days of change detection is investigated by radiative transfer model simulations and observations. Successive SAR observations with the same look angle from wet and dry days are available from the ERS1 and ERS2 tandem mission. We therefore concentrate on the ERS C-band SAR. Furthermore, this study will focus on forest, because interception and backscatter of forests are well studied, and thus data are available for validation. A problem arises, as direct observations of rain storage are not available due to the almost complete lack of measurement techniques. The validation is therefore carried out indirectly by estimating forest wetness with a standard hydrological model. These simulations are used to relate the forest backscatter change with the forest wetness change and thus to estimate the potential of SAR to measure large-scale vegetation wetness and rainfall interception.

MODELS

Interception

Three phases are generally distinguished in the interception process. The first phase starts at the beginning of rainfall. A dense canopy intercepts most raindrops, and relatively few fall through the canopy without contact. The canopy can retain only a certain amount of rainfall, the so-called maximum storage capacity S_{max}. The second phase starts when stored rain exceeds S_{max} and excessive water runs off to the ground. The third, drying phase starts when rainfall stops.

Following Deardorff (1978), interception is modeled by considering the canopy as a bucket, which is filled by precipitation and emptied by evaporation. The bucket flows over if S_{max} is reached. Assuming a closed canopy that intercepts all raindrops, variations in storage S are calculated by

$$\frac{\partial S}{\partial t}=P-R-E \tag{1}$$

where P is the precipitation flux, E is the evaporation flux from the wet canopy, and R is the runoff flux from the canopy, all in mm h^{-1}. Run off occurs only if S exceeds S_{max}. The value of S_{max} is calculated by assuming that each leaf or needle is covered with a 0.2-mm-thick water film on one side (Dickinson, 1984), so

$$S_{max}=0.2\mathrm{LAI} \tag{2}$$

where LAI is the one-sided leaf area index and S_{max} is in mm rain. The evaporation flux is (Deardorff, 1978)

$$E=\left(\frac{S}{S_{max}}\right)^{2/3}E_p \tag{3}$$

where E_p is the potential evaporation, which is calculated with the Penman–Monteith formula with zero canopy resistance (Monteith, 1965). This formula is based on the energy budget and is a function of the aerodynamic resistance, humidity, temperature and available energy. The aerodynamic resistance is calculated from the windspeed and the aerodynamic roughness. The latter is estimated from the aerodynamic roughness for heat (Lankreijer et al., 1993).

Radar Backscatter

Radar backscatter of forest is simulated by the three-layer UTA Radiative Transfer Canopy Model (UTART-Can) (Karam et al., 1992, 1995). The input parameters of the model are the density, size, orientation, and dielectric constant of trunks, branches, and leaves or needles, grouped in horizontal layers. The forest is in our case schematized as two separate, continuous layers: a canopy layer and a trunk layer. The canopy layer consists of leaves or needles, and branches. The trunk layer is located under the canopy layer and consists of only trunks. As second-order scattering contributes significantly only on cross-polarized backscattering (vertical to horizontal polarization and vice versa) (Karam et al., 1992), and the ERS–SAR is only vertical polarized, the model is restricted to simulate first-order scattering effects. In other words, the incoming radar wave is reflected and transmitted by the vegetation cover. Backscattering from the soil occurs either directly or via double bounce via trunks or other canopy elements; in these cases the vegetation cover attenuates the radar wave two times.

The scattering and attenuation in the canopy depends on the dielectric constant, size, orientation, and

density of each vegetation cover element (leaf or needle, branch, and trunk). The dielectric constant of a single element is determined mainly by its water content. This water is free or bound to organic molecules, with both forms of water having different dielectric constants. A single, effective dielectric constant of each element is calculated with the Debye–Cole dual-dispersion model (Ulaby and El-Rayes, 1987), which is based on the assumption that the inhomogenities inside an element are smaller than common radar wavelengths (X-, C-, L-, and P-bands; i.e., 3–67 cm). As a consequence, each element can be considered as a homogeneous medium and thus the effective dielectric constant is obtained by volumetric averaging of the dielectric constants of both forms of water. So, the basic form of the Debye–Cole dual-dispersion model is

$$\varepsilon=\varepsilon_r+v_f\varepsilon_f+v_b\varepsilon_b \tag{4}$$

where ε is the dielectric constant and v the volume fraction. The subscripts r, f, and b denote a relatively unimportant residual component due to the solid matter of the canopy element, the free water inside the element, and the bound water inside the element, respectively. The volume fractions and the residual dielectric constant are calculated as a function of the gravimetric water content M_g with the following empirical equations (Ulaby and El-Rayes, 1987):

$$v_f=M_g(0.55M_g-0.076) \tag{5a}$$

$$v_b=4.64M_g^2(1+7.36M_g^2) \tag{5b}$$

$$\varepsilon_r=1.7-0.74M_g+6.16M_g^2 \tag{5c}$$

The dielectric constants of the free water and bound water are calculated with the Debye and Cole–Cole equations (Ulaby and El-Rayes, 1987) and resulted in 73.2–j28.8 and 9.8–j5.5, respectively.

As mentioned in the introduction, most of the stored rain is retained on the leaf or needle surface. The influence of this water is estimated by adapting the effective dielectric constant and the thickness of the leaves or radius of the needles in the radiative transfer model. This adaptation will be described in the following paragraph.

Equation (2) denotes that a leaf or needle can retain the equivalent of a 0.2-mm-thick water film. This water is stored as droplets or as a film. The film thickness or the size and distance between the droplets will be small compared with common radar wavelengths. Following the Debye–Cole dual-dispersion model, stored rain is considered part of the homogeneous leaf. We assume that all stored rain is free water. Consequently, the volume fraction of stored rain v_s can be added to the free-water term of Eq. (4):

$$\varepsilon=\varepsilon_r+(v_s+v_f)\varepsilon_f+v_b\varepsilon_b \tag{6}$$

As well as changing the dielectric constant, storage also changes the dimensions of the leaf or needle. The thickness of a wet leaf is calculated by assuming that stored rain forms a homogeneous film on the leaf. Additionally, stored water is assumed to be distributed homogeneous over all leaves. Deciduous leaves are schematized as disks. The thickness of a wet deciduous leaf is now related to storage by

$$d=d_{lf}+d_s \tag{7a}$$

with

$$d_s=\frac{S}{\mathrm{LAI}} \tag{7b}$$

where d is the thickness, lf denotes the leaf, and s the water layer. A needle is modeled as a cylinder. The radius of a wet needle is obtained by adding the volume of the stored water (V_s) to the volume of the needle:

$$\pi r_w^2 l=\pi r_d^2 l+V_s \tag{8a}$$

with

$$V_s=0.5\cdot 2\pi r_d l\frac{S}{\mathrm{LAI}} \tag{8b}$$

which results in

$$r_w=\sqrt{r_d^2+r_d\frac{S}{\mathrm{LAI}}} \tag{8c}$$

where r_w and r_d are the radius of the wet and the dry needle, respectively, and l is the length of the needle. The factor $2\pi r_d l$ in Eq. (8b) is the surface area of a needle and 0.5 is brought into this equation as the storage is a function of the one-sided LAI, which in the case of needles is half the surface area.

STUDY SITE AND DATA

Figure 1a shows the area of interest (AOI), a parallelogram of 20 km×85 km near the center of the Netherlands. The large forest in the south is the Veluwe, ±350 km^2 mixed temperate forest on sandy soil. The function of this forest is partly production forest and partly nature reserve. The most recent forest stands of the Veluwe were planted around 1900, and the oldest already existed in the Middle Ages. Most forest stands are dominated by coniferous species (spruce, larch, and pine: *Picea*, *Larix*, and *Pinus* spp.) and have a small fraction (<10%) of large (>15 m) deciduous trees such as oak, birch, and beech (*Quercus*, *Betula*, and *Fagus* spp.) (Ten Houte de Lange, 1977). LAI maps of the Veluwe do not exist. Published plot measurements of the LAI at the Veluwe range from 2.8 (Dolman et al., 1998) up to 11 (Bouten et al., 1996). A field survey showed that these plots are extremes. The averaged LAI is estimated to be 5.

The SAR image pairs of the AOI were acquired by the ERS1 (first day) and ERS2 (second day) on 7 and 8 September 1995 and 25 and 26 May at 10:30 UMT

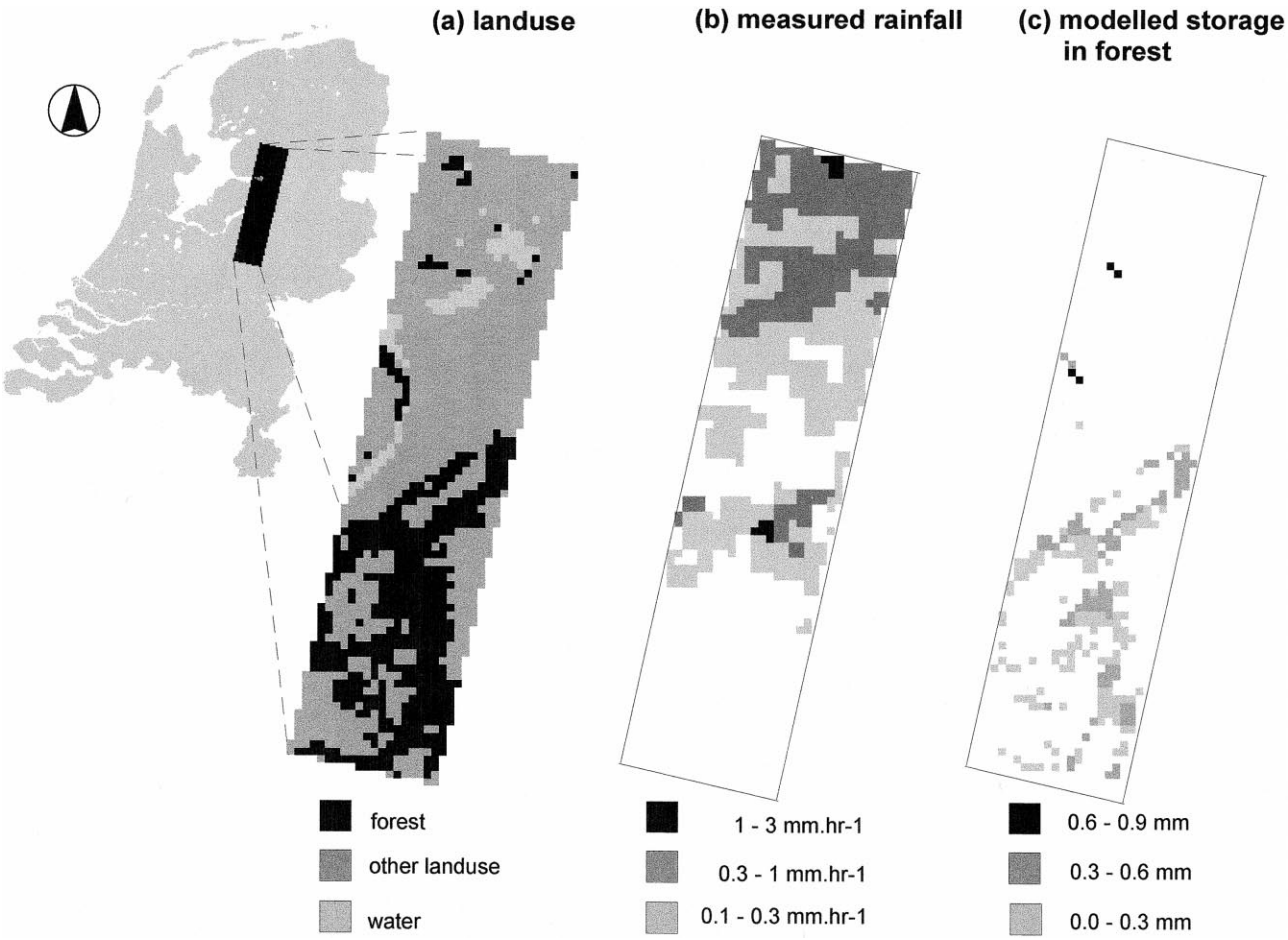

Figure 1. The location of the area of interest near the centre of the Netherlands, showing (a) land use and (b) the precipitation rate at 8 September during the moment of ERS overpass; and (c) the modeled storage in the pixels with a subgrid fraction forest >75% at the same time. Note that all pixels with rain and 2 km around the shower are excluded from further analysis.

(12:30 local summer time). Both SAR's operate at C-band vv-polarization, and the ERS1 and ERS2 orbit and look angle were identical. A fractional land-use map on a 1-km×1-km grid was taken from a GIS database (Anonymous, 1997). Precipitation rates originate from the rain radar of the Royal Dutch Meteorological Organization. Figure 1b is an example of a (resampled) rain radar image. With a time resolution of 15 minutes and a spatial resolution of 2.5 km, the rain radar recorded a number of precipitation rate classes: 0.1–0.3, 0.3–1, 1–3, 3–10, and 10–30 mm h^{-1}. The whole AOI is located within a 100-km distance of the rain radar. Detailed meteorological and hydrological observations were carried out in two forest stands. One location was situated in a pine stand in the center of the Veluwe, the other in a poplar (*Populus* spp.) forest 20 km west from the center of the AOI. The measurement sites and equipment used are described in Elbers et al. (1996) and Dolman et al. (1998). The measured parameters include precipitation, run off, available energy, humidity, and windspeed. Soil moisture at 3 cm depth was also measured at the site within the Veluwe. Table 1 sums some parameter values at the moment of satellite overpass, to which we will refer to afterward.

To simulate the backscatter sensitivity to forest wetness with the radiative transfer model, suitable input data must be chosen. An exact parameterization of the forest in the radiative transfer simulations was not tried because the forest structure varies within the measurement grid of 1 km×1 km. Instead, backscatter sensitivity to wetness was simulated for a few characteristic forest stands. As most of the Veluwe is covered with coniferous species, a dense and a sparse coniferous forest are simulated. To show the difference between a coniferous and a deciduous forest, the backscatter sensitivity from an average deciduous stand was also simulated. The forest types are a low coniferous black spruce stand with LAI 1.5, a coniferous white spruce stand with LAI 9.1, and a deciduous poplar stand with LAI 3.6. The structural parameters of these stands are given in Table 2. The gravimetric water content of the needles and leaves was set at 60%, and the water content of the wooden ele-

Table 1. Relevant Characteristics of the Observed Area at the Moment of Satellite Overpass

Date	*7 September*	*8 September*	*25 May*	*26 May*
shower top (km)	—	5.7	3.9	4.5
surface windspeed ($m.s^{-1}$)	3.3	4.5	2.8	4.1
surface wind direction (°)	146	108	254	244
soil moisture at 3 cm (%)	14.9	15.0	20.5	21.1

ments at 50%. This are normal values for healthy trees in the Netherlands (Hoekman et al., 1995). The maximum storage is assumed to be the equivalent of a 0.2-mm-thick water layer on each leaf or needle. The structural parameters of the soil were in all simulations set equal. The surface roughness had a rms height of 1 cm, and a correlation length of 4 cm. The volumetric moisture content of the soil was set to 20%, a value close to the maximum soil moisture measured during the satellite overpasses (Table 1).

DATA PROCESSING

Data were processed on a 1 km×1 km grid. Pixels with a subgrid fraction forest larger than 75% were selected with the GIS database. It was assumed that these pixels were fully covered with forest. Spatial variation in precipitation input was obtained from rain radar measurements. These rain radar images were resampled to the model grid with nearest neighbor sampling, and the precipitation rate classes were replaced by the logarithmic mean of the class concerned. Other input data were assumed to be spatially constant. The potential evaporation rate was estimated by first calculating the local potential evaporation rate at the two locations with known meteorological data, which were then averaged. If measurements were available from one location only, these were applied. This occurred at 7 September before 13:30 UMT due to device failure. For the remainder of the time, the correlation between the evaporation rates at the two locations is 0.86 and the mean difference 0.02 mm h^{-1}. Spatial averaging of evaporation rate therefore introduces only minor deviations in the resulting storage, which is in agreement with Ghan et al. (1997). The spatial distribution of S_{max} does have on the contrary a large influence on modeled storage (Eltahir and Bras, 1993). Measurements of S_{max} within the test area vary between 0.5 (Lankreijer et al., 1993) and 2.5 mm (Bouten et al., 1996). The influence of S_{max} was therefore analyzed by using the values 0.5, 1.5, and 2.5 mm.

The backscatter change of the ERS1 and ERS2 image pairs were derived by first calculating the linear

Table 2. Forest Structure Parameters Used in the Radiative Transfer Model Simulations[a]

	Black Spruce	*White Spruce*	*Balsam Poplar*
Canopy layer			
Canopy-layer height	5.1	14.7	10.1
Leaves/needles			
LAI	1.5	9.1	3.6
Mean length (cm)	0.8	1.6	6.8
Mean thickness/diameter (cm)	0.1	0.1	0.03
Orientation	$0.5\sin(\varphi)$	$0.5\sin(\varphi)$	$0.5\sin(\varphi)$
Maximum water layer (mm)	0.2	0.2	0.2
Primary branches			
Mean length (m)	0.62	1.13	2.0
Mean diameter (cm)	1.81	2.24	1.50
Density (branches/m^3)	1.31	2.37	6.69
Orientation	$\sin^9(\theta-30°)$	$\sin^4(\theta)$	$\sin^9(\theta+60°)$
Secondary branches			
Mean length (m)	0.39	0.57	1.0
Mean diameter (cm)	0.81	1.04	0.75
Density (branches/m^3)	1.31	2.37	6.69
Orientation	$\sin^9(\theta)$	$\sin^9(\theta)$	$\sin^9(\theta+60°)$
Trunk layer			
Trunk-layer height	5.1	16.7	20.1
Trunks			
Mean height (m)	5.1	16.7	20.1
Mean diameter (cm)	6.5	21.3	22.5
Stem density (stems/m^2)	0.137	0.0654	0.106

[a] The forest is schematised as a canopy layer above a trunk layer. These parameters are based on Rignot et al. (1994).

backscatter coefficient σ^0 from ERS PRI-products with the ERS SAR Toolbox, based on the calibration procedure of Laur et al. (1997). The calibrated images were next georeferenced, averaged to the 1 km×1 km grid and converted to dB. The calibration includes compensation of ADC saturation effects, as the ERS2 ADC saturation is significantly decreased compared with the ERS1 ADC saturation. Compensation of ADC saturation increased the backscatter of the ERS1 on average with 0.2 dB over the selected forest pixels. Another source of false backscatter changes might be rainfall, as it attenuates C-band backscatter by a few percent (Ulaby et al., 1981, p. 3). The rain radar detected rainfall at a maximum of 5.7 km above the surface (Table 1). Assuming a look angle of 23° and a shower height of 5 km, this rain could distort the radar signal up to 2 km behind the shower. Pixels with rain as well as pixels up to 2 km around the shower were therefore excluded from the analyses. After this data selection, 117 and 119 forest pixels were analyzed from the May and September image pairs. The resulting accuracy is claimed to be within ±0.4 dB (Laur et al., 1997).

RESULTS

Simulated Sensitivity of C-band Radar to Vegetation Wetness

The simulated sensitivity to intercepted rain for three different forest types is shown in Figures 2a–c. The backscatter from the primary and secondary branches are added and only the backscatter terms that contribute more than −30 dB are shown. Figure 2a shows the backscatter sensitivity from the sparse black spruce stand to storage. The most important terms contributing to the backscatter are the soil and the branches. Dry needles are relatively unimportant. The backscatter from the trunks and via the soil–trunks, soil–needles, and soil–branches are small. When needles become wet, the backscatter of needles increases with 7.8 dB at the maximum storage. The backscatter of wet needles is still an unimportant fraction of the total backscatter. However, wetness not only causes a backscatter increase from needles, it also enhances attenuation by needles. As a result, the backscatter from the soil and branches decreases with −3.0 dB and −1.3 dB, respectively, and the total backscatter of the black spruce forest stand decreases with −2.2 dB.

The same processes, increased backscatter of leaves and decreased backscatter from branches and soil due to attenuation, occur in the other forest stands, but, as will be seen, the significance of these processes depends on the forest stand parameters. Figure 2b shows the simulated sensitivity of the dense white spruce stand. The backscatter from the branches is the most important term in the dry state. The backscatter from the soil and the trunks is negligible. The backscatter from needles increases due to wetness with 6.0 dB, and the backscatter from branches decreases with −3.1 dB. As a consequence, the needles become the most important scatters in the wet white spruce stand, and the total backscatter increases with +1.1 dB. Figure 2c shows the backscatter sensitivity of the poplar stand to wetness. The total backscatter is dominated by the backscatter of leaves. This increases with 4.7 dB at the maximum storage. The total backscatter increases with 4.4 dB when leaves get wet.

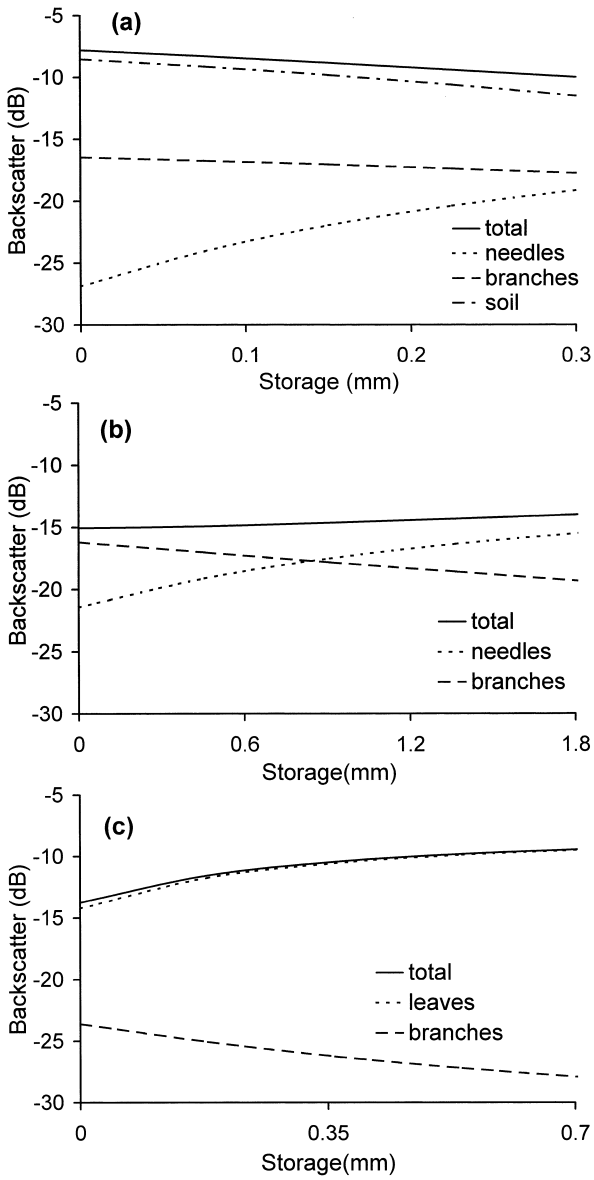

Figure 2. Modeled backscatter of (a) sparse black spruce stand, (b) dense white spruce stand, and (c) poplar stand as a function of the rain storage on the needles and leaves. Shown are all backscatter contributions which exceed −30 dB. With increasing storage the backscatter from needles and leaves increases while the backscatter from the soil and branches decreases.

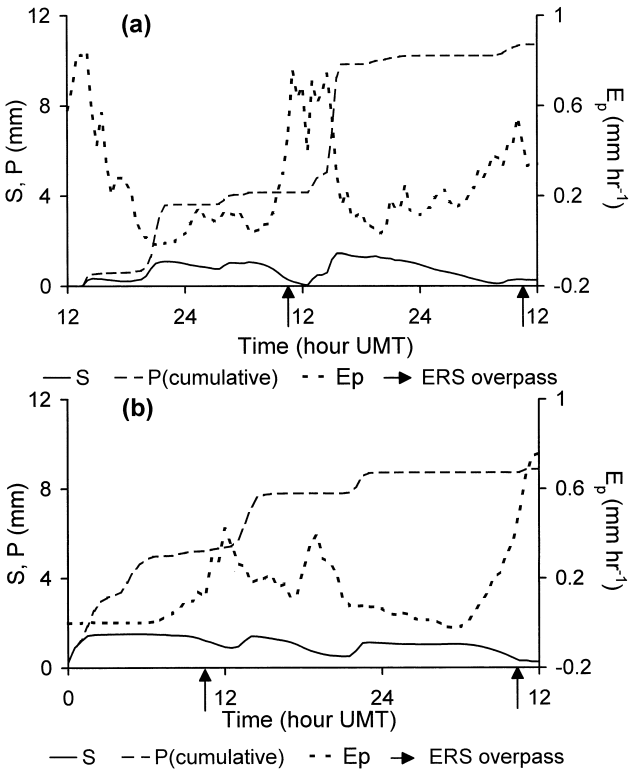

Figure 3. Areally averaged cumulative precipitation (mm), potential evaporation rate (mm h^{-1}) and rainfall storage (mm) modeled assuming S_{max} is 1.5 mm (a) in September, and (b) in May.

This is slightly less than the increased backscatter from the leaves due to enhanced attenuation of the other backscatter terms. These simulations show that the backscatter sensitivity of a forest to wetness depends on the relative contribution of the leaves or needles (i.e., on the forest structure). The difference in backscatter between a completely dry and wet forest may vary between −2 dB and 4 dB.

Rain Storage at the Moment of Satellite Overpass

Rain storage is modeled as a spatial and temporal variable. An example of the spatial heterogeneity of the modeled storage assuming an S_{max} of 1.5 mm is shown in Figure 1c. Note that Figure 1b shows the rainfall at the same time. It rains in the center and the north of the AOI. Because the rain passed the AOI from south to north, the south of the AOI is already partly dry. The storage varies between 0.0 and 0.5 mm. The spatial differences result from the rainfall amount and the drying time since the last rainfall.

Figure 3a shows the spatially averaged storage modeled with an S_{max} of 1.5 mm in September as a function of time. The figure also contains the main driving parameters: rainfall and potential evaporation flux. The potential evaporation flux shows a clear day–night rhythm: low evaporation fluxes in night time and high evaporation fluxes in day time. Moderate rainfall saturated the canopy in the first afternoon. Some drizzle fell in the evening. Although evaporation rate was low during the night, still a significant part of the canopy dried during this night. The stored water starts to evaporate rapidly after dawn. It rained intensely the following afternoon, but as the night was dry a large fraction of the storage evaporated before dawn. That same morning, drizzle with bright clearings passed the Veluwe, so vegetation was partly wetted again. The figure shows that the ERS1 and 2 overpasses were both in the drying phase of the canopy. The situation in May was quite different; see Figure 3b. It rained almost continuously the first night. Combined with a low evaporation rate this resulted in a high storage in the morning. It rained again the following afternoon and evening, and additionally dew occurred (indicated by a negative potential evaporation). Due to the high evaporation rate, most of the stored water evaporated quickly in the morning. The ERS1 and ERS2 overpasses were again both in the drying phase, but the amount of storage was much higher during the first overpass.

Table 3 shows the range of storage modeled with the different values of S_{max} at the moments of satellite overpass in the AOI. S_{max}=0.5 mm is regarded as the lower limit, and S_{max}=2.5 mm as the upper limit of expected storage capacity. A large S_{max} causes more rain accumulation, and the canopy stays wet longer. For all values of S_{max}, this table shows that the canopy was dry (or at the most half wet) on both days in September, while the canopy was almost saturated during the first overpass and significant drier during the second overpass in May.

Observed Backscatter Change

Figure 4 shows the relation between backscatter change and storage change calculated with S_{max}=1.5. A positive value means more backscatter, or a wetter canopy on the first day, and a negative value the inverse. The scatter on the *x*-axis (storage) is caused by variations in precipitation rate and in drying time after the rain events. The September data show distinct spatial storage change, but the variations are always less than 1/3 of the maximum storage capacity. The averaged storage change is insignificant. The averaged backscatter change in September is also insignificant, and 93% of the pixels have a backscatter change less than ±0.4 dB, the expected measurement noise. The September observations therefore agree with the simulations when changes in rain storage are small. In May, the storage was large on the first day and small on the second. The backscatter change varied between +0.7 dB and +2.5 dB, with an average of +1.3 dB. As most of the Veluwe consist of rather dense mixed forests, this observation is within the range of simulated sensitivity of dense forests.

Table 3. Rain storage at the time of satellite overpass from the pixels used in the analysis as a function of the model parameter S_{max}[a]

	7 September			*8 September*			*25 May*			*26 May*		
S_{max} *(mm)*	*mean (mm)*	*min. (mm)*	*max. (mm)*	*mean (mm)*	*min. (mm)*	*max. (mm)*	*mean (mm)*	*min. (mm)*	*max. (mm)*	*mean (mm)*	*min. (mm)*	*max. (mm)*
0.5	0.0	0.0	0.0	0.1	0.0	0.3	0.2	0.1	0.3	0.0	0.0	0.0
1.5	0.3	0.0	0.5	0.3	0.1	0.6	1.2	1.0	1.3	0.2	0.0	0.4
2.5	0.7	0.1	1.4	0.7	0.3	1.0	2.1	1.2	2.3	0.8	0.1	1.3

[a] Shown are the parameters describing the spatial variability of rain storage.

DISCUSSION

The feasibility of measuring large-scale forest wetness by using C-band SAR backscatter changes between successive days was empirically tested. The observed sensitivity to rainfall storage agrees with modeled sensitivity. The significance of this result is analyzed, based on a discussion of the underlying models.

The maximum modeled backscatter change due to wetness (+4 dB) is slightly higher than the maximum observed backscatter increase mentioned in the introduction (+3 dB) and observed in this study (+2.5 dB). It will be qualitatively discussed whether this might be caused by a systematic deviation of the model. The first assumptions concern the rain storage at the scale of the leaf. Equation (2) assumes that all rain is stored on leaves and needles. However, rain may also be stored on branches and trunks. In case of coniferous species, one could even imagine that relatively much rain is stored as small drops at the transition of the twig to the needle. The storage on needles and leaves and the resulting backscatter from these is therefore overestimated. As the sensitivity to wetness of the backscatter from trunks and branches will be small due to the small relative volume change and consequently small dielectric constant change, this overestimation of the backscatter from the leaves will be only partly compensated by increased backscatter from trunks and branches. The stored rain is next considered as free water, while a small part of the stored rain might be bound to the surface of the leaf or needle. The water adheres to this surface due to the physical processes of surface tension differences between the water and the leaf surface and friction (Horton, 1919). As these bonds are weak compared with chemical bonds, this assumption causes only a slight overestimation of the modeled sensitivity. At a slightly larger scale, modeling the needles and the small branches in case of coniferous forest as independent entities is a rough approach. Needles may be regularly ordered at distances smaller than the radar wavelength (5.7 cm), and backscattering interaction between the needles might therefore occur. The next set of assumptions discussed applies to the scale of the canopy. The storage is assumed to be homogeneously distributed in the canopy. Model calculations indicated that the upper canopy dries fater than the lower canopy (Watanabe and Mizutani, 1996). Thus, suppose that the upper canopy is dry while the lower canopy is still wet. The backscatter change of the upper canopy will be zero while the lower canopy backscatter will partly be attenuated by the upper parts. This assumption would therefore result in an overestimation of the sensitivity. The canopy is also assumed to be continuous. In reality, there will be gaps in the canopy, even in dense forests. As a result, part of the backscatter will arise from the soil and the backscatter sensitivity to leaf wetness will further decrease. Thus, most model assumptions probably result in an overestimation of the sensitivity of radar backscatter to water storage. The simulated backscatter sensitivity is therefore regarded as the maximum sensitivity.

Figure 4. Backscatter change versus canopy storage change modeled with S_{max} is 1.5 mm. A positive value means a higher storage or a stronger backscatter on the first day. The canopy was almost dry during both September overpasses. The first day was wet and the second day was dry during the May overpasses.

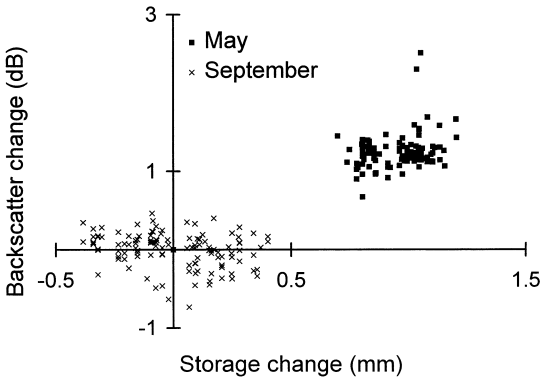

The SAR observations are indirectly validated on ground truth via modeled storage. The modeled storage depends strongly on the precipitation rate, the maximum storage capacity, and the evaporation rate between the end of the rain and the moment of observation. The accuracy of precipitation rate derived from rain radar is low (Stewart et al., 1998), just like the accuracy in the value of S_{max} and the evaporation rate from a wet canopy (Klaassen et al., 1998). If, as before the first overpass in May, it rained intensely for several hours, then the can-

opy is saturated with rain, and the uncertainty in precipitation rate is not important. In that case, the uncertainty in actual storage is determined mainly by the uncertainty in S_{max}. On the other hand, if small showers occur and the canopy does not saturate, as before both September overpasses, then the uncertainty in S_{max} hardly influences the actual storage. In that case, the uncertainty in storage is determined by the precipitation rate and evaporation rate uncertainty. Given the uncertainty in ground truth, it is concluded that the September data are not useful to test the SAR observations and the May data are useful only for a qualitative comparison of the SAR observations.

Although the observed backscatter changes in May can be explained by wetness changes, the backscatter may have been changed by other causes. The significance of some often-mentioned causes for temporal change in backscatter (Hobbs et al., 1998; Saich and Borgeaud, 1998) is therefore evaluated for the present situation. The backscatter depends on the forest structure, which might change due to altering wind. On the Beaufort scale, the wind changed between the May image pair from windforce 2 to windforce 3 (Table 1). The wind direction stayed almost constant. According to the description of the Royal Dutch Meteorological Organization, small branches start to move at Beaufort windforce 4. It is therefore assumed that the wind did not cause any relevant backscatter changes. Furthermore, backscatter depends on soil moisture and soil moisture might change after rainfall. Soil moisture was measured at 3 cm depth at the measurement site within the Veluwe. The measurements in May took place in a rainy period. The soil was wetter the second day (+0.6%; see Table 1) than the first day, due to rainfall between the moments of ERS overpass. This higher soil moisture would result in a higher backscatter on the second day. The vegetation was wet the first day and dry the second day. This would cause an increased backscatter on the first day. We observed the latter, and this is therefore attributed to rain storage in the canopy.

CONCLUSION AND RECOMMENDATIONS

We examined the feasibility of detecting forest canopy rain storage with change detection between successive C-band SAR images. According to simulations, the sensitivity of radar backscatter to forest wetness is strongly dependent on the type of forest. The modeled sensitivity ranged from −2 to +4 dB. Due to model assumptions, this sensitivity is the maximum sensitivity. The relative contribution of the leaves or needles to the total backscatter is the parameter that governs whether backscatter will increase or decrease with increasing storage of rain. Backscatter change observations were made by the ERS tandem mission and compared with modeled wetness change as ground truth. The accuracy of ground truth is only qualitatively fair, due to uncertainties in input parameters. The observed backscatter change between a wet and a dry forest varied from +0.7 dB to 2.5 dB, which agrees with the simulations. It is therefore concluded that C-band short-time change detection is a feasible approach to discriminate between wet and dry forest.

A disadvantage of satellite observations appeared in the September dataset, when both observations dealt with a partially wet forest and measurements could not be used to detect changes in rain storage. This example shows that at least one dry observation is desired to monitor rain storage, which reduces the number of suitable observations. Another disappointing result is that the backscatter sensitivity to canopy wetness strongly depends on forest structure. ERS–SAR observations alone are therefore not sufficient to quantify rain storage in forests. Additional information on forest structure is needed for that purpose.

The forest structure might be retrieved by multiple wavelength radar remote sensing. An additional advantage of multiple wavelength observations is that the sensitivity to storage is wavelength dependent, and therefore a combination of wavelengths could perform more accurate. Finally, using modeled wetness as ground truth introduces uncertainties. It is therefore recommended to use direct local measurement of rain storage as ground truth.

This study was sponsored by the Dutch Space Research Organization (SRON). The ERS tandem images were provided by ESA, the rain radar data by R. Jilderda from the Royal Dutch Meteorological Organization (KNMI), and the detailed meteorological and hydrological data by E. Moors and A. J. Dolman from the Staring Centre. H. Laur from ESA/ESRIN provided a copy of the SAR ToolBox. We would like to thank B. Hoenders, J. Delvigne, and two anonymous referees for their comment on the manuscript.

REFERENCES

Ahern, F. J., Leckie, D. J., and Drieman, J. A. (1993), Seasonal changes in relative C-band backscatter of northern forest cover types. *IEEE Trans. Geosci. Remote Sens.* 31:668–680.

Anonymous (1997), *LKN, Landscape Ecological Atlas of The Netherlands*, University of Wageningen, the Netherlands, CD-ROM.

Bergen, K. M., Dobson, M. C., Pierce, L. E., and Ulaby, F. T., (n.d.), *Effects of Within Season Dielectric Variations on Terrain Classification Using Sir-C/X-Sar*, University of Michigan, Radiation Laboratory, Unpublished.

Bernard, R., and Vidal-Madjar, D. (1989), C-band radar cross section of the Guyana rain forest, possible use as a reference target for spaceborne radars. *Remote Sens. Environ.* 27:25–36.

Blöschl, G., and Sivapalan, M. (1995), In *Scale Issues in Hydrological Modelling*. A review. (J. D. Kalma et al., Eds.), John Wiley & Sons, Chichester, UK, Chap. 1. pp. 9–68.

Bouten, W., Schaap, M. G., Aerts, J., and Vermetten, A. W. M. (1996), Monitoring and modelling canopy water storage amounts in support of atmospheric deposition studies. *J. Hydrol.* 181:305–321.

Choudhury, B. J., DiGirolamo, Susskind, J., Darnell, W. L., Gupta, S. K., and Asrar, G. (1998), A biophysical process-based estimate of global land surface evaporation using satellite and ancillary data. II. Regional and global patterns of seasonal and annual variations. *J. Hydrol.* 205:186–204.

Deardorff, J. W. (1978), Efficient prediction of ground surface temperature and moisture with inclusion of a layer of vegetation. *J. Geophys. Res.* 83:1889–1903.

Dickinson, R. E. (1984), Modeling evatranspiration for three-dimensional global climate models. In *Climate Processes and Climate Sensitivity*, Geophys. Monogr. 29, American Geophys. Union, Washington, DC, pp. 58–72.

Dobson, M. C., Pierce, L., McDonald, K., and Sharik, T. (1991), Seasonal change in radar backscatter from mixed conifer and hardwood forest in northern Michigan. In *Proc. IGARSS 91*, Espoo, Finland, pp. 1121–1124.

Dolman, A.J., and Gregory, D. (1992), The parameterization of rainfall interception in GCMs. *Q. J. R. Meteorol. Soc.* 188: 445–467.

Dolman, A. J., Moors, E. J., Elbers, J. A., and Snijders, W. (1998), Evaporation and surface conductance of three temperate forests in the Netherlands. *Ann. Sci. For.* 55:255–270.

Elbers, J. A., Dolman, A. J., Moors, E. J., and Snijders, W. (1996), *Hydrology and Water Management of Forests in the Netherlands, Phase 2: Measurements and the First Results* (in Dutch). Staring Centre Report 333.2, Wageningen, The Netherlands.

Eltahir, E. A. B., and Bras, R. L. (1993), A description of rainfall interception over large areas. *J. Climate* 6:1002–1008.

Gash, J. H. C. (1979), An analytical model of rainfall interception by forest. *Q. J. R. Meteorol. Soc.* 105:43–55.

Gates, W. L., Henderson-Sellers, A., Boer, G. J., Folland, C. K., Kitoh, A., McAvaney, B. J., Semazzi, F., Smith, N., Weaver, A. J., and Zeng, Q. C. (1995), In *Climate Change 1995, The Science of Climate Change* (J. T. Hougton et al., Eds.), Cambridge University Press, Cambridge, UK, pp. 279–284.

Ghan, S. J., Liljegren, J. C., Shaw, W. J., Hubbe, J. H., and Doran, J. C. (1997), Influence of subgrid variability on surface hydrology. *J. Climate* 10:3157–3166

Hobbs, S. E., Ang, W., and Seynat, C. (1998), Wind and rain effects on SAR backscatter from crops. In *2nd Int. Workshop on the Retrieval of Bio- and Geo-physical Parameters from SAR Data for Land Applications* (M. Borgeaud and T. D. Guyenne, Eds.), ESA/ESTEC, Noordwijk, The Netherlands, pp. 185–189.

Hoekman, D. H., van der Linden, M., and van der Sanden, J. J. (1995), In *Application of ERS-1 SAR Data in Agriculture and Forestry* (G. J. A. Nieuwenhuis and W. W. L. van Rooij, Eds.), BCRS, Delft, The Netherlands, pp. 105–121.

Horton, R. E. (1919), Rainfall interception. *Mon. Weather Rev.* 47:603–623.

Karam, M. A., Fung, A. K., Lang, R. H., and Chauhan, N. S. (1992), A Microwave scattering model for layered vegetation. *IEEE Trans. Geosci. Remote Sens.* 30:767–783.

Karam, M. A., Amar, F., Fung, A. K., Mougin, E., Lopes, A., LeVine, D. M., and Beaudoin, A. (1995), A microwave polarimetric scattering model for forest canopies based on vector radiative transfer theory. *Remote Sens. Environ.* 53:16–30.

Klaassen, W., Linden, M. van der, and Ballast, A. (1997), SAR sensing of vegetation wetness: the first results. In *3rd ERS Symposium on Space at the Service of Our Environment*, Florence, Italy, pp. 103–106.

Klaassen, W., Bosveld, F., and Water, E. de (1998), Water storage and evaporation as constituents of rainfall interception. *J. Hydrol.* 212–213:36–50

Lankreijer, H. J. M., Hendriks, M. J., and Klaassen, W. (1993), A comparison of models simulating rainfall interception of forests. *Agric. For. Meteorol.* 64:187–199.

Laur, H., Bally, P., Meadows, P., Sanchez, J., Schaettler, B. and Lopinto, E. (1997), Derivation of the backscattering coefficient σ^0 in ESA ERS SAR PRI products. In *ESA, Document ES-TN-RS-PM-HL09*, Issue 2, Rev. 4.

Linacre, E., and Geerts, B. (1997), *Climates and Weather Explained*, Routledge, London, New York.

Monteith, J. L. (1965), Evaporation and environment. *Symp. Soc. Exp. Biol.* 19:205–234.

Noilhan, J., Lacarrère, P., Dolman, A. J., and Blyth, E. M. (1997), Defining area-average parameters in meteorological models for land surfaces with mesoscale heterogeneity. *J. Hydrol.* 190:302–316.

Pitman, A. P., Henderson-Sellers, A., and Yang, Z. L. (1990), Sensitivity of regional climates to localised precipitation in global models. *Nature* 346:734–737.

Pulliainen, J. T., Heiska, K., Hyyppä, J., and Hallikainen, M. (1994), Backscattering properties of boreal forest at the C- and X-bands. *IEEE Trans. Geosci. Remote Sens.* 32: 1041–1050.

Rignot, E., Way, J. B., McDonald, K., Viereck, L., Williams, C., Adams, P., Payne, C., Wood, W., and Shi, J. (1994), Monitoring of environmental conditions in Taiga Forest using ERS-1 SAR. *Remote Sens. Environ.* 49:145–154.

Rutter, A. J., Kershaw, K. A., Robins, P. C., and Morton, A. J. (1971), A predictive model of rainfall interception in forests. 1. Derivation of the model from observations in a plantation of Corsican pine. *Agric. Meteorol.* 9:367–384.

Saich, P., and Borgeaud, M. (1998), Interpreting agricultural crop signatures from Flevoland, 1993–1994. In *2nd Int. Workshop on the Retrieval of Bio- and Geo-physical Parameters from SAR Data for Land Applications* (M. Borgeaud and T. D. Guyenne, Eds.) ESA/ESTEC, Noordwijk, The Netherlands, pp. 175–184

Schowengerdt, R.A. (1983), *Techniques for Image Processing and Classification in Remote Sensing*, New York, Academic Press, pp. 249.

Sellers, P. J., Dickinson, R. E., Randall, D. A., Betts, A. K., Berry, J. A., Collatz, G. J., Denning, A. S., Mooney, H. A., Nobre, C. A., Sato, N., Field, C. B., and Henderson-Sellers, A. (1997), Modeling the exchanges of energy, water, and carbon between continents and the atmosphere. *Science* 275:502–509.

Shuttleworth, J. W. (1988), Evaporation from Amazonian rain forest. *Proc. R. Soc. London Ser. B* 233:321–346.

Stewart, J. B., Engman, E. T., Feddes, R. A., and Kerr, Y. H. (1998), Scaling up in hydrology using remote sensing: summary of a workshop. *Int. J. Remote Sens.* 19(1):181–194.

Ten Houte de Lange, S. M. (1977), *Report from the Veluwe Investigation* (in Dutch), Centre for Agricultural Publications and Agricultural Documentation (PUDOC), Wageningen, The Netherlands, 263 pp.

Ulaby, F. T., Moore, R. K., and Fung, A. K. (1981), *Microwave Remote Sensing, Active and Passive. Vol. I. Fundamentals and radiometry*, Artech House, Norwood, UK.

Ulaby, F. T., and EL-Rayes, M. A. (1987), Microwave dielectric spectrum of vegetation. Part II. Dual-dispersion model. *IEEE Trans. Geosci. Remote Sens.* 25:550–557.

Watanabe, T., and Mizutani, K. (1996), Model study on micrometeorological aspects of rainfall interception over an evergreen broad-leaved forest. *Agric. For. Meteorol.* 80:195–214.

Way, J., Paris, J., Kasischke, E., Slaughter, C., Viereck, L., Christensen, N., Dobson, M. C., Ulaby, F., Richards, J., Milne, A., Sieber, A., Ahern, F. J., Simonett, D., Hoffer, R., Imhoff, M., and Weber, J. (1990), The effect of changing environmental conditions on microwave signatures of forest ecosystems: preliminary results of the March 1988 Alaskan aircraft SAR experiment. *Int. J. Remote Sens.* 11:1119–1144.